The Journal of Chemical Physics

Phase separation in binary fluid mixtures with symmetric and asymmetric Schmidt numbers: A DPD study

Cite as: J. Chem. Phys. **150**, 234903 (2019); https://doi.org/10.1063/1.5088540
Submitted: 11 January 2019 . Accepted: 29 May 2019 . Published Online: 19 June 2019

Harinadha Gidituri, V. S. Akella, Srikanth Vedantam, and Mahesh V. Panchagnula

The Journal of Chemical Physics ARTICLE scitation.org/journal/jcp

Phase separation in binary fluid mixtures with symmetric and asymmetric Schmidt numbers: A DPD study

Cite as: J. Chem. Phys. 150, 234903 (2019); doi: 10.1063/1.5088540
Submitted: 11 January 2019 • Accepted: 29 May 2019 •
Published Online: 19 June 2019

Harinadha Gidituri,[1] V. S. Akella,[1,a)] Srikanth Vedantam,[2] and Mahesh V. Panchagnula[1]

AFFILIATIONS

[1] Department of Applied Mechanics, Indian Institute of Technology Madras, Chennai 600 036, India
[2] Department of Engineering Design, Indian Institute of Technology Madras, Chennai 600 036, India

[a)] Electronic mail: sathishakella@gmail.com

ABSTRACT

We investigate the effect of the Schmidt number (Sc) on phase separation dynamics of two immiscible fluids in a two-dimensional periodic box using dissipative particle dynamics. The range of Sc investigated spans liquid-liquid separation processes. Phase separation is characterized by a domain size $r(t)$, which typically follows a power law t^{β} in time t, where β is a characteristic exponent corresponding to the coarsening mechanism at play. The phase separation dynamics is studied for strongly (deep quench) separating mixtures. We consider cases of critical ($\phi \sim 0.5$) and off-critical ($\phi < 0.5$) mixtures of fluids A and B for both $Sc_A = Sc_B$ and $Sc_A \neq Sc_B$. In all cases, the growth dynamics slow down with the increasing Schmidt number of either fluid. We observe the power law exponent $\beta = 0.5$ for symmetric ($Sc_A = Sc_B$) critical mixtures and $\beta = 0.33$ for all other cases. However, for off-critical mixtures, the exponent is 0.33 irrespective of the Schmidt number ratio of the two fluids. We explain these results from an analysis of the competition between diffusive effects vis-á-vis dynamical forces.

I. INTRODUCTION

Phase separation processes are relevant to many physico-chemical systems such as alloys,[1,2] polymers,[3,4] and liquid crystals.[5–8] Understanding the microscopic effects in such systems is essential to designing new generation materials. The phase separation process of a binary fluid mixture, when quenched to below the mixture's critical point, is usually characterized by the domain size $r(t)$. It is widely known that $r(t) \sim t^{\beta}$, where t is time. The value of the exponent β is an important parameter that characterizes the dynamical process and is dimensionality dependent. For 3D low volume fraction binary mixtures ($\phi < 0.1$), the domains coarsen via droplet coalescence[9] with a predicted exponent of $\beta = 1/3$ in early stages. At later stages, the evaporation-condensation mechanism causes domain coarsening with $\beta = 1/3$. On the other hand, for 3D critical binary mixtures ($\phi \sim 0.5$), the phase separation begins via interface diffusion (predicted $\beta = 1/3$) with bicontinuous structures which are the characteristic of spinodal decomposition.[9] At later times, hydrodynamic flow causes the breakup of these interconnected structures, tubular structures, leading to rapid coarsening with $\beta = 1$.

By contrast, for two-dimensional (2D) off-critical binary mixtures, the coarsening proceeds via droplet coalescence followed by evaporation-condensation with the corresponding exponents $\beta = 1/2$ and $\beta = 1/3$. Note that the growth law scaling for the evaporation-condensation mechanism is independent of dimensionality, i.e., $\beta = 1/3$. In critical mixtures, the phase separation occurs via spinodal decomposition with bicontinuous structures (predicted $\beta = 1/2$) followed by droplet coalescence with $\beta = 1/2$. It is important to note that the same coarsening mechanisms are operative both in 3D and 2D but with different scaling laws. These predictions were verified both in simulations[10–13] and experiments.[14,15]

Many simulation methods have been employed for simulating the phase separation process. These methods range from Molecular Dynamics (MD) at the microscale; Lattice Boltzmann Method (LBM), Lattice Gas Automata (LGA), and Dissipative Particle Dynamics (DPD) at the mesoscale; and Navier-Stokes (NS) equations at the continuum scale. Dissipative Particle Dynamics (DPD) is a coarse-grained method which has some computational advantages over the other mesoscale and microscale methods in modeling the hydrodynamics of complex fluids. In a DPD simulation,

each DPD particle is a model for a collection of several fluid molecules. This method was first introduced by Hoogerbrugge and Koelman,[16] which was later developed through the extensive investigations on the applicability to different physical problems.[17,18] Due to the soft-repulsive nature of the interparticle potential, larger time and length scales are accessible with DPD when compared with Molecular Dynamics (MD). There are two reasons why one should be concerned about the dynamic properties of fluids, such as viscosity and diffusivity, while modeling the binary phase separation process using the DPD method. First, the phase separation dynamics strongly depends on viscosity and diffusivity of the fluids.[19,20] For example, the mechanism for phase separation can either be diffusion dominated or advection dominated or both depending on the dynamical properties of the individual fluids. Second, the momentum transport is slow due to the soft-core repulsive potential of the DPD method which is in the same order of the diffusive transport.

A dimensionless number which quantifies the relative transport of momentum and mass diffusion is the Schmidt number (Sc) which is defined as the ratio of viscosity to diffusivity ($Sc = \frac{\nu}{D}$). Typical values of the Schmidt number in a standard DPD fluid are of $\mathcal{O}(1)$, which is not typical of liquids. The competing effects in a typical liquid-liquid phase separation process are dictated by interface forces which are responsible for dynamical and diffusive effects. In other words, $Sc \sim \mathcal{O}(1)$, which corresponds to a gaseous phase where hydrodynamic behavior is suppressed. However, for most soft matter systems with liquid as a medium, the corresponding Sc numbers are much higher [$Sc \sim \mathcal{O}(10^3)$]. Therefore, it is necessary to increase the Schmidt number to model the hydrodynamic behavior of the liquids accurately. The dynamic properties of DPD fluids, such as viscosity (ν) and diffusivity (D), can be tuned to increase Sc, which plays an important role in determining the underlying mechanism of the phase separation process.[21–23] To the best of our knowledge, there are only a few studies on the effect of viscosity asymmetry on the phase separation of binary fluid mixtures in the reported literature.[19,20,24,25] In addition, it is quite often the case in binary phase separation that the dynamic properties, such as viscosity and diffusivity, of each of the individual fluids will be very much different.[26–28] Apart from that it is advantageous to study any physical phenomenon in terms of nondimensional numbers to scale up a process from a small scale to large scale. Toward this end, we investigate the effect of symmetrical and asymmetrical dynamical properties, such as viscosity (ν) and diffusivity (D), of individual fluids A and B on the binary phase separation process in terms of their ratio, the Schmidt number.

The organization of the paper is as follows. In Sec. II, a brief overview of the finite-sized DPD method, the simulation parameters, the calculation of dynamic properties of the DPD fluid, the Schmidt number (Sc), and the domain size are presented. In Sec. III, we compare the results of phase separation behavior for different combinations of Schmidt numbers Sc for the investigation of fluids A and B by computing the temporal evolution of domain size. Finally, we present the conclusions of the study in Sec. IV.

II. COMPUTATIONAL METHODOLOGY: FDPD

In this section, we briefly outline the Finite Sized Dissipative Particle Dynamics (FDPD) method originally proposed by Pan *et al.*[29] In this formulation, each FDPD particle is considered to be a coarse-grained model consisting of several fluid molecules. Initially, the simulation domain is seeded with N such FDPD particles with an average number density ρ per unit volume. Each FDPD particle is chosen to have a mass m_i ($i = 1, \ldots, N$), each of radius R_i and corresponding mass moment of inertia I_i. These particles satisfy the laws of conservation of both linear and angular momenta. These conservation equations are

$$m_i \frac{d\mathbf{v}_i}{dt} = \mathbf{f}_i, \tag{1a}$$

$$I_i \frac{d\boldsymbol{\omega}_i}{dt} = -\sum_{j \neq i} \lambda_{ij} \mathbf{r}_{ij} \times \mathbf{f}_{ij}, \tag{1b}$$

where $\mathbf{v}_i$ and $\mathbf{f}_i = \sum_{j \neq i} \mathbf{f}_{ij}$ are velocity and force, respectively, on the ith particle. $\mathbf{f}_{ij}$ is the effective force exerted on the ith particle by a neighboring jth particle at a distance $\mathbf{r}_{ij} = \mathbf{r}_i - \mathbf{r}_j$, and $\boldsymbol{\omega}_i$ is the angular velocity. The torque exerted by each particle is weighted by $\lambda_{ij} = R_i/(R_i + R_j)$, where R_i and R_j are particle radii of ith and jth particles, respectively. The position, linear, and angular velocities of each FDPD particle are resolved componentwise by the forces and moments exerted by the neighboring particles within a certain cut-off distance r_c. The pairwise force $\mathbf{f}_{ij}$ is a sum of four forces each of different nature, viz., (i) a central conservative ($\mathbf{f}_{ij}^C$), (ii) a translational dissipative ($\mathbf{f}_{ij}^T$), (iii) a rotational dissipative ($\mathbf{f}_{ij}^R$), and (iv) a stochastic or random ($\mathbf{f}_{ij}^S$). Mathematically,

$$\mathbf{f}_{ij} = \mathbf{f}_{ij}^C + \mathbf{f}_{ij}^T + \mathbf{f}_{ij}^R + \mathbf{f}_{ij}^S. \tag{2}$$

The central conservative force is always repulsive and acts along a line connecting centers of particles i and j and is given by

$$\mathbf{f}_{ij}^C = \alpha_{ij} \Gamma(r_{ij}) \hat{\mathbf{e}}_{ij}, \tag{3}$$

where α_{ij} is the repulsion interaction coefficient, $r_{ij} = |\mathbf{r}_{ij}|$, and $\hat{\mathbf{e}}_{ij} = \mathbf{r}_{ij}/r_{ij}$ is a unit vector. A linear weight function $\Gamma(r_{ij})$ is chosen such that the conservative force is purely repulsive and vanishes linearly at a limiting value $r_{ij} = r_c$. The conservative weight function, $\Gamma(r_{ij})$, is given by

$$\Gamma(r_{ij}) = \begin{cases} 1 - \frac{r_{ij}}{r_c}, & \text{if} \quad r_{ij} \leq r_c, \\ 0, & \text{if} \quad r_{ij} > r_c. \end{cases} \tag{4}$$

The translational dissipative force will have both central and non-central components, which are given by

$$\mathbf{f}_{ij}^T = -\gamma_{ij}^{\parallel} w^D(r_{ij})(\mathbf{v}_{ij} \cdot \hat{\mathbf{e}}_{ij})\hat{\mathbf{e}}_{ij} - \gamma_{ij}^{\perp} w^D(r_{ij})[\mathbf{v}_{ij} - (\mathbf{v}_{ij} \cdot \hat{\mathbf{e}}_{ij})\hat{\mathbf{e}}_{ij}], \tag{5}$$

respectively. Here, $\gamma_{ij}^{\parallel}$ and $\gamma_{ij}^{\perp}$ are the central and shear components of dissipation coefficients. The relative velocity $\mathbf{v}_{ij} = \mathbf{v}_i - \mathbf{v}_j$ between the particles in both directions is reduced by the translational frictional force. Similarly, the rotational dissipative force is assumed to be of the form

$$\mathbf{f}_{ij}^R = -\gamma_{ij}^{\perp} w^D(r_{ij})[\mathbf{r}_{ij} \times (\lambda_{ij}\boldsymbol{\omega}_i + \lambda_{ji}\boldsymbol{\omega}_j)]. \tag{6}$$

A stochastic Brownian force, which accounts for the lost degrees of freedom due to the coarse graining, is given by

$$\mathbf{f}_{ij}^{S}dt = w^{R}(r_{ij})[\sigma_{ij}{}^{\parallel}\mathrm{tr}[d\mathbf{W}_{ij}]\frac{1}{\sqrt{D}}\mathbf{1} + \sqrt{2}\sigma_{ij}{}^{\perp}d\mathbf{W}_{ij}{}^{A}]\cdot\hat{\mathbf{e}}_{ij}, \quad (7)$$

where $\mathbf{f}_{ij}^{S}dt$ is the net impulse due to the random force during an infinitesimal time step dt. $D = 2$ for two-dimensional simulations, $\mathrm{tr}[d\mathbf{W}_{ij}]$ is the trace of the symmetric independent Wiener increment matrix $d\mathbf{W}_{ij}$, and $d\mathbf{W}_{ij}{}^{A}$ is its antisymmetric part. To satisfy the fluctuation dissipation theorem, the random and dissipation coefficients are correlated by $\sigma_{ij}{}^{\parallel} = \sqrt{2k_BT\gamma_{ij}{}^{\parallel}}$ and $\sigma_{ij}{}^{\perp} = \sqrt{2k_BT\gamma_{ij}{}^{\perp}}$. The choice of these parameters provides an implicit thermostat so that the FDPD simulations are performed at constant temperature. Here, $w^{D}(r_{ij})$ and $w^{R}(r_{ij})$ are weight functions which physically determine the relative strengths of the dissipative and random forces, respectively, and are related due to fluctuation-dissipation theorem (FDT). We use the generalized weight function for the dissipative force following Fan *et al.*,[30]

$$w^{D}(r_{ij}) = [w^{R}(r_{ij})]^{2} = \begin{cases} \left(1 - \frac{r_{ij}}{r_c}\right)^{s}, & \text{if} \quad r_{ij} \leqslant r_c, \\ 0, & \text{if} \quad r_{ij} > r_c. \end{cases} \quad (8)$$

Here, s is the exponent in the weight function and Eq. (8) ensures that the fluctuation-dissipation theorem (FDT) is satisfied. A generalized form of the dissipative weight function vs r/r_c for various values of exponent s is shown in Fig. 1. For values $s < 1$, the weight function is concave and the dissipative interaction between particles is weighted more heavily in comparison with the standard quadratic weight function ($s = 2.0$). These differences in the form of the weight function affect the effective diffusivity as well as the viscosity, thereby the Schmidt number. The velocity-Verlet algorithm is used to integrate the particle positions with a time step of $\Delta t = 0.001$. It must be emphasized that the choice of Δt must be dealt with utmost care as the wrong choice could yield unphysical results. For example, in the present system, if the time step is large ($\Delta t \sim 0.01$), the system shows arresting behavior, which is an artifact. We varied Δt systematically to eliminate the Δt dependence on the simulating system and arrived at a value of 0.001. The factor dt in the stochastic/random force can be explained by assuming the random force as the Wiener process.

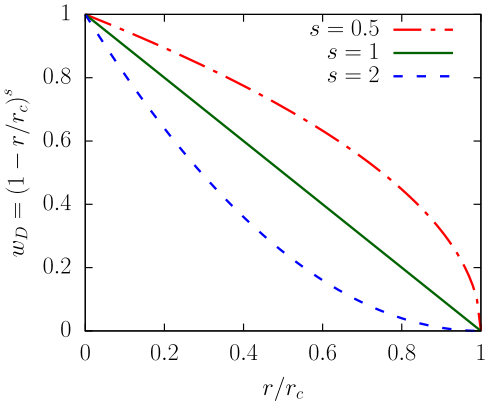

FIG. 1. Generalized dissipative force weighting functions.

This dt factor is to remove the time step dependence on the physical process.[18]

A. Simulation parameters and calculation of dynamic properties

As mentioned before, Sc determines the relative importance of momentum and mass diffusion. In the current context, it plays an important role in phase separation dynamics. Simulation parameters such as the dissipative coefficient (γ), cut-off radius (r_c), and weight-exponent (s) can be tuned to increase the Schmidt number in order to produce the physically consistent hydrodynamic behavior. Different approaches have been proposed by several researchers[22,23,30] to accomplish this end. In the present work, we have chosen to vary the dissipative coefficient (γ) and weight exponent (s) systematically to vary the Schmidt number.

We are interested in characterizing the effect of Sc on the binary separation process. At the start of the simulation, particles of both A-type and B-type are well-mixed by arranging them randomly in the computational domain. The number densities for both the fluids are set to $\rho_A = \rho_B = 3/2$. The repulsion coefficient α_{ij} is different for the different species interaction. In our simulations, we have chosen $\alpha_{AA} = \alpha_{BB} = 25$ for A–A and B–B interactions and $\alpha_{AB} = 50$ for the A–B interaction, which corresponds to a deep quench separation regime.[31] The random and dissipative coefficients in the central and shear directions $\sigma_{ij}{}^{\parallel} = \sigma_{ij}{}^{\perp}$ and $\gamma_{ij}{}^{\parallel} = \gamma_{ij}{}^{\perp}$ are chosen to satisfy the fluctuation-dissipation theorem, which in turn keeps the system temperature k_BT at a constant value of 1. Different values considered in the present work for the central and shear components of the dissipative coefficients are presented in Table I. The central and shear components of the dissipative components are taken to be equal and are represented by $\gamma_{ij}{}^{\parallel} = \gamma_{ij}{}^{\perp} = \gamma_{ij}$.

The dynamical behavior in the phase separation of binary fluid systems is strongly influenced by the viscosity of the pure fluids as well as viscosity difference (or ratio) between A and B fluids. Since the phase separation process is dominated by the discontinuity in viscosity across the fluid domains, it is essential to model the correct viscosity at the fluid-fluid interface. The concept of defining the different repulsion coefficient α_{ij} for like (A–A or B–B) and unlike (A–B) particles is well-known in the modeling of immiscible binary fluids using the DPD method. One can use a similar strategy in modeling multiviscosity systems. The dissipative coefficient (γ) for like particles (A–A or B–B) gives the viscosity of pure A and B fluids.

TABLE I. Schmidt number variation as a function of exponent of dissipative force weight function s and dissipative force coefficient γ.

s	γ	Sc
2.0	4.5	1.0
2.0	22.5	2.5
2.0	45.0	5.0
2.0	90.0	13.0
0.5	4.5	3.3
0.5	22.5	43.0
0.5	45.0	160.0
0.5	90.0	635.0

But, it is not straightforward to define the dissipative coefficient (γ) for unlike particles (A–B). Visser *et al.*[32] proposed a model for multiviscosity systems using the DPD method. We closely follow their work in modeling the viscosity at a fluid-fluid interface, viz., between A and B fluids. In their work, they have taken the dissipative coefficient for A and B interactions γ_{AB} as a harmonic mean of pure fluid dissipative coefficients γ_{AA} and γ_{BB}. Pure fluid viscosities for different values of the dissipative coefficient (γ) were calculated and validated using the planar Poiseuille flow method.[21,33] A parabolic velocity profile $u = u_{\max}\left(1-\frac{y^2}{h^2}\right)$ based on the Navier-Stokes equation is fitted to simulation results of the Poiseuille flow. The maximum velocity $u_{\max}$ can be obtained from the fitting, and the dynamic viscosity of the fluid can be calculated using $u_{\max} = \frac{\rho g h^2}{2\mu}$, where g is the steady external force and h is the distance from the center to the wall of the channel. In our simulations, we have chosen four different values for γ_{AA} and γ_{BB}. They are given by 4.5, 22.5, 45.0, and 90.0 corresponding to successively high viscosities. We confirmed that the fluid is Newtonian by obtaining a parabolic velocity profile[30] for different combinations of the values of weight function exponent (s), dissipative coefficient (γ), and external force (g) and our results are in agreement with Kasiteropoulou *et al.*[34] The 2-dimensional diffusion coefficient D of pure fluids is calculated using mean square displacement (MSD) of particles after long time. Mathematically, it can be written as

$$D = \lim_{t\to\infty} \frac{1}{4N\Delta t} \sum_{i=1}^{N} \langle [r_i(t) - r_i(0)]^2 \rangle. \tag{9}$$

Based on the values of kinematic viscosity ν and diffusivity D, the Schmidt number ($Sc = \frac{\nu}{D}$) is calculated and tabulated in Table I for different values of γ.

B. Domain size calculation

Beginning from a well-mixed condition, the two phases begin to separate due to interfacial force. This process results in the formation of domains of one fluid embedded in another. The domain size (of, say, species A) exhibits different power law behavior $r(t) \propto t^{\beta}$, where the exponent β varies depending on the coarsening mechanism. In our case, we have calculated the domain size $r(t)$ using the structure factor[35] $S(k, t)$, which is the spatial Fourier transform of the density map of the phase separating mixture at time t.

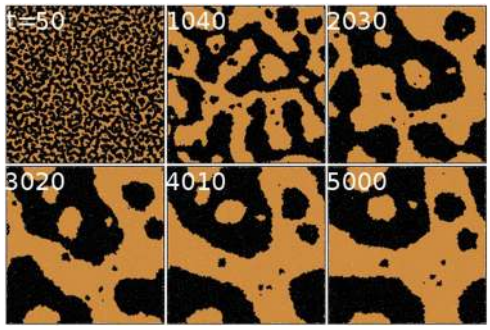

FIG. 2. Phase separation morphologies of two fluids A and B at different times with critical area fraction (ϕ = 0.5) at Sc_A = 635 and Sc_B = 635. Color code: fluid A—brown and fluid B—black. Multimedia view: https://doi.org/10.1063/1.5088540.1

The calculation of $r(t)$ is as follows:

$$S(k = |\mathbf{k}|, t) = \frac{1}{N}\left[\left(\sum_{i=1}^{N} \cos(\mathbf{k}\cdot r_i)\right)^2 + \left(\sum_{i=1}^{N} \sin(\mathbf{k}\cdot r_i)\right)^2\right], \tag{10}$$

$$\mathbf{k} = \frac{2\pi}{L}(i\boldsymbol{e_x} + j\boldsymbol{e_y}), \quad \text{where} \quad i,j = 0, \pm1, \pm2, \pm3, \ldots. \tag{11}$$

Here, N is the number of particles, r_i is the position vector of the ith particle, $\mathbf{k}$ is the wave vector, and L is the size of the domain,

$$r(t) = 2\pi \frac{\sum_{|\mathbf{k}|=0}^{|\mathbf{k}|_{\text{cut}}} S(|\mathbf{k}|, t)}{\sum_{|\mathbf{k}|=0}^{|\mathbf{k}|_{\text{cut}}} |\mathbf{k}| S(|\mathbf{k}|, t)}. \tag{12}$$

The value of k_{cut} is chosen such that the largest domain size obtained had a length scale less than $2\pi/k_{\text{cut}}$.

III. RESULTS AND DISCUSSION

In the present work, we are interested in understanding the effect of the Schmidt number (Sc) on the phase separation process. We study this systematically for critical mixtures (ϕ = 0.5) and off-critical mixtures (ϕ < 0.5) for different combinations of Schmidt numbers of fluids A and B. Note that in all the simulations performed, the value of s is the same for both the fluids A and B, either 2.0 or 0.5. All the simulations are performed in a two-dimensional

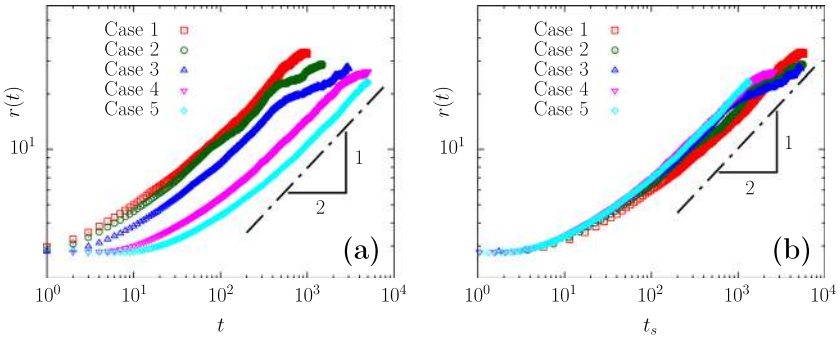

FIG. 3. (a) Domain size $r(t)$ vs simulation time t. (b) Domain size $r(t)$ vs $t_s \sim Dt$, where D is the diffusion constant of either of the pure fluids A and B. Collapse of $r(t)$ for different Sc values indicates that the coarsening mechanism is the same for all the cases which is interface diffusion. Case 1: $Sc_A = Sc_B \sim 1$, Case 2: $Sc_A = Sc_B \sim 2.5$, Case 3: $Sc_A = Sc_B \sim 13$, Case 4: $Sc_A = Sc_B \sim 160$, and Case 5: $Sc_A = Sc_B \sim 635$ with critical area fraction (ϕ = 0.5).

(2D) periodic box of dimensions $L_x \times L_y = 100 \times 100$ with a total of 3×10^4 particles (both of fluids A and B) randomly arranged (initially) in the simulation box. The quench protocol for a simulation is as follows. At $t = 0$, a homogeneous mixture of fluids A and B fills the simulation domain, and instantaneously, the value of the repulsion coefficient α_{AB} is set to 50 (corresponds to a deep quench), which drives the system into phase separation. For box sizes greater than 100×100, the simulation results are invariant. We checked the invariance based on the growth exponent (β). Therefore, a box size of 100×100 was used for all the cases in this work. All the results produced in this work are averaged over a minimum of 5 trials. We validated all our results with the DPD formulation against the findings of Novik and Coveney.[10]

A. Critical mixtures

In this section, we discuss phase separation dynamics of critical mixtures of fluids of same and different Schmidt numbers.

1. Equal Sc fluids ($Sc_A = Sc_B$)

The phase separation in these cases proceeds always via spinodal decomposition. The domains of the individual fluids are interconnected, and domain coarsening occurs through interface diffusion. The domain size $r(t)$ scales as $t^{1/2}$ as theorized by Miguel *et al.*[9] in 2D through dimensional arguments. Our simulations can be construed as ending at intermediate times (prior to break up of interconnected structures) since we are interested in the time range when bicontinuous structures are present. Our reported exponents are valid for this regime. In order to ascertain that the corresponding exponent is not an artifact of our choice of box size, we performed simulations with varying system sizes for sufficiently long times. The exponent in all cases for intermediate times yielded $\beta = 1/2$. At later times, the interconnected structures could break up and can coarsen either by droplet coalescence or by evaporation-condensation[36] with $\beta = 1/2$ or $\beta = 1/3$, respectively (both in 2D and 3D), as reported by Lamorgese and Mauri[11,12] from their investigations of phase separation dynamics of binary mixtures using a diffuse-interface model. Figure 2 shows the time evolution of phase separation morphology for fluids A and B with $Sc_A = Sc_B \sim 635$.

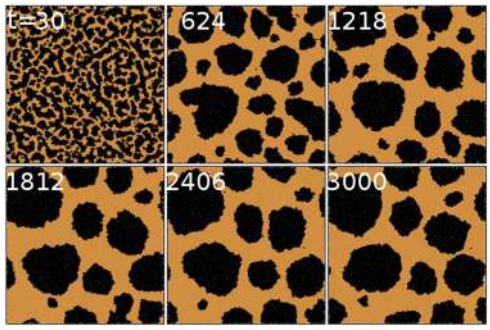

FIG. 4. Phase separation morphologies of two fluids A and B at different times with critical area fraction ($\phi = 0.5$) at $Sc_A \sim 635$ and $Sc_B \sim 3$. Color code: fluid A—brown and fluid B—black. Multimedia view: https://doi.org/10.1063/1.5088540.2

From the morphological evolution, we conclude that the phase separation proceeds predominantly through the coarsening of interconnected domains irrespective of the magnitudes of the viscosities of individual fluids. However, an increase in viscosity decreases the diffusivity of the individual fluids, thereby delaying the phase separation.

Figure 3(a) shows the domain size $r(t)$ as a function of simulation time for different Schmidt numbers. These results are in agreement with the expected scaling (dotted-dashed line) $r(t) \sim t^{1/2}$. Figure 3(b) is the domain size $r(t)$ vs $t_s \sim Dt$, where D is the diffusion coefficient of either fluid A or B (note that $D_A = D_B$ in this case). This procedure synchronizes different coarsening time scales. Rescaling the time axis results in the collapse of $r(t)$ for different Schmidt numbers, suggesting that diffusion is the dominant mechanism causing domain coarsening.

2. Unequal Sc fluids ($Sc_A \neq Sc_B$)

The asymmetry in viscosity across the fluid interface greatly modifies the phase separation process. First of all, interface diffusion is *not* the dominant mechanism for domain coarsening. This is

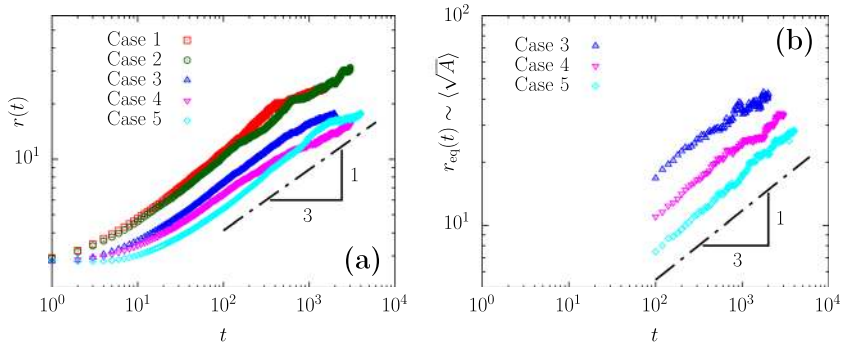

FIG. 5. (a) Domain size $r(t)$ vs simulation time t. (b) Domain size $r_{eq}(t)$ vs t. r_{eq} is the average equivalent radius of all the domains in the simulation box and defined as $r_{eq}(t) \sim \langle\sqrt{A(t)}\rangle$, where A is the area of a domain and angular brackets represent ensemble average over a simulation box. Case 1: $Sc_A \sim 5$ and $Sc_B \sim 1$, Case 2: $Sc_A \sim 13$ and $Sc_B \sim 1$, Case 3: $Sc_A \sim 160$ and $Sc_B \sim 3$, Case 4: $Sc_A \sim 635$ and $Sc_B \sim 3$, and Case 5: $Sc_A \sim 635$ and $Sc_B \sim 43$ with critical area fraction ($\phi = 0.5$). Cases 1 and 2 are omitted in (b) due to poor statistics.

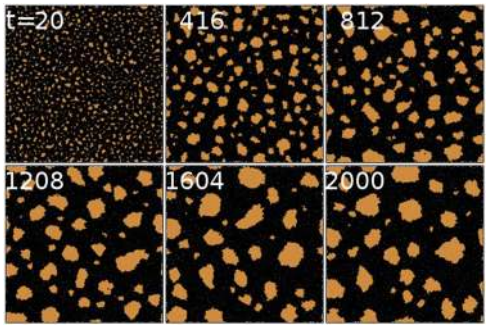

FIG. 6. Phase separation morphologies of two fluids *A* and *B* at different times with off-critical area fraction (ϕ = 0.25) at $Sc_A \sim 43$ and $Sc_B \sim 635$. Color code: fluid A—brown and fluid B—black. Multimedia view: https://doi.org/10.1063/1.5088540.3

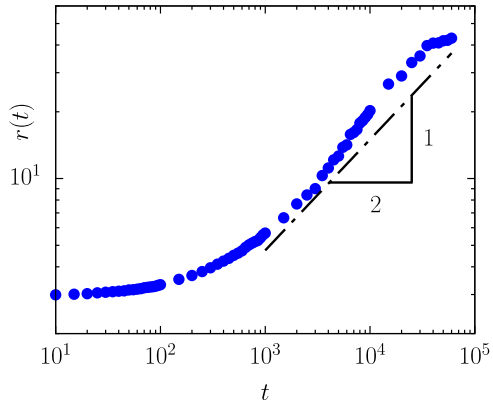

FIG. 8. Domain size $r(t)$ vs simulation time t at interfacial tension between fluids A and B, $\Gamma_{AB} = 14.14 \pm 0.16$, corresponding to the DPD parameters $s = 2$, $\phi = 0.25$, $\rho = 6$, $\alpha_{AA} = \alpha_{BB} = 12.5$ and $\alpha_{AB} = 50$, and $\gamma_{AA} = \gamma_{BB} = \gamma_{AB} = 4.5$. In comparison with case 2 of Fig. 7 where $Sc_A/Sc_B = 1$ and $\Gamma_{AB} = 2.44 \pm 0.43$.

evident from the morphological evolution of fluid domains as shown in Fig. 4. Clearly, the system shows interconnected/bicontinuous structures at early times but quickly transforms into a stage where disconnected domains of the low viscosity fluid (fluid *B*) diffuse around in a continuum of the high viscosity fluid (fluid *A*). Upon careful inspection, we found that the domain coarsening occurs primarily via Brownian coagulation/droplet coalescence. Figure 5(a) is the plot of domain size $r(t)$ vs t. In this case, $r(t) \sim t^{1/3}$ (dotted-dashed line). Dimensional arguments[9] suggest that the droplet coalescence mechanism leads to a $t^{1/2}$ scaling law in 2D, which is clearly in disagreement with our observation. We would like to mention that the Lifshitz-Slyozov-Wagner (LSW) mechanism (evaporation-condensation or Ostwald ripening)[37–39] yields a $t^{1/3}$ in 2D; however, we see *no* evidence of Ostwald ripening in our system. In deriving the scaling law for droplet coalescence,[9] it was assumed that the droplets are far apart and that two drops encounter each other through diffusive motion. However, in the present case where $\phi = 0.5$, the droplets are packed densely and the hydrodynamics developed due to the asymmetry in viscosity across the fluid interfaces greatly modify the coarsening mechanism. We speculate that the coupling between hydrodynamics and diffusion affects the droplet coalescence mechanism, which results in $t^{1/3}$ scaling for domain size. Our observations are in agreement with Luo *et al.*[19] They observed both $t^{1/2}$ and $t^{1/3}$ scaling for unequal viscosity fluids at $\phi = 0.5$. In addition, $t^{1/2}$ scaling is observed for higher individual viscosities and $t^{1/3}$ for lower individual viscosities while maintaining the ratio of viscosities of individual fluids at 4:1. These results suggest that the coupling between hydrodynamics and diffusion affects droplet coalescence behavior and therefore the power in the scaling law.

B. Off-critical mixtures

We performed off-critical mixture simulation at $\phi = 0.25$ with $Sc_A \sim 43$ and for different values of Sc_B. In all the cases, fluid *A* forms isolated domains in fluid *B* and domains coarsen via Brownian coagulation/droplet coalescence. Figure 6 shows the morphological evolution of fluid domains at $Sc_A \sim 43$ and $Sc_B \sim 635$. Figure 7(a) shows the domain size $r(t)$ as a function of simulation time t and the observed scaling (dotted-dashed line) of $t^{1/3}$, which is in disagreement with the proposed scaling of $t^{1/2}$ for droplet coalescence. Again, we see *no* evidence for the LSW mechanism under these conditions which follows as $t^{1/3}$ law.

We present arguments based on our simulations in support of the observed power law. The domain size scaling law derived for droplet coalescence assumes[40] that the droplets are sparsely populated and $\tau_\sigma \ll \tau_D$. The first time scale $\tau_\sigma \sim \frac{\rho v l}{\sigma}$ is known as the fusion time scale, i.e., time taken for the fusion of droplets to be

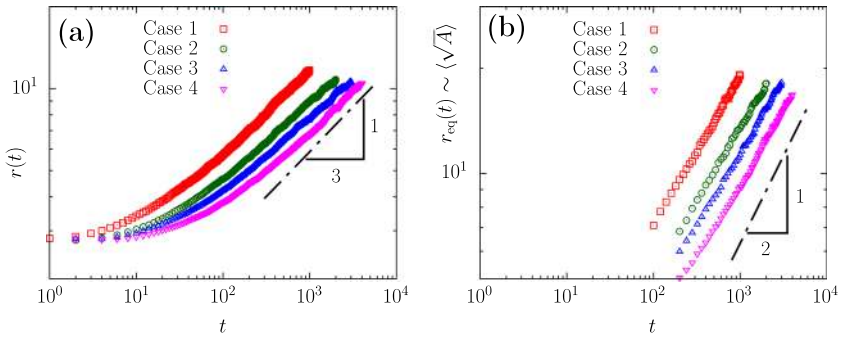

FIG. 7. (a) Domain size $r(t)$ vs simulation time t. (b) Domain size $r_{eq}(t)$ vs t. r_{eq} is the average equivalent radius of all the domains in the simulation box and defined as $r_{eq}(t) \sim \langle\sqrt{A(t)}\rangle$, where $A(t)$ is the area of a domain and angular brackets represent ensemble average over a simulation box. Case 1: $Sc_A \sim 43$ and $Sc_B \sim 3$, Case 2: $Sc_A \sim 43$ and $Sc_B \sim 43$, Case 3: $Sc_A \sim 43$ and $Sc_B \sim 160$, and Case 4: $Sc_A \sim 43$ and $Sc_B \sim 635$) with off-critical area fraction ($\phi = 0.25$).

TABLE II. Summary of measured and predicted growth exponents and the corresponding coarsening mechanism for critical ($\phi \sim 0.5$) and off-critical ($\phi < 0.5$) mixtures at equal and unequal Schmidt number values of individual fluids *A* and *B*.

ϕ	Sc	β from r(t)	β from $r_{eq}(t)$	β predicted	Coarsening mechanism
0.5	$Sc_A = Sc_B$	0.5	...	0.5	Interface diffusion
0.5	$Sc_A \neq Sc_B$	0.33	0.33	...	Droplet coalescence[a]
<0.5	$Sc_A = Sc_B$	0.33	0.5	0.5	Droplet coalescence
<0.5	$Sc_A \neq Sc_B$	0.33	0.5	0.5	Droplet coalescence

[a] Modified by the hydrodynamics caused by the viscosity jump across the fluid interface.

completed, where ρ is the density of droplet fluid, ν is the kinematic viscosity of the continuous fluid, l is size of the drop, and σ is the interfacial tension between the droplet fluid and the continuous fluid. The time scale $\tau_D \sim \frac{l^2}{D}$ corresponds to diffusion, i.e., time taken for a droplet to encounter another droplet through diffusive motion, where D is the diffusion coefficient of the droplet in the continuous fluid. We speculate that the assumption $\tau_\sigma \ll \tau_D$ breaks down for the choice of our simulation parameters. In other words, these time scales could be comparable. In order to rationalize these results, we present calculations of domain size using image processing. We calculated the domain size as $r_{eq}(t) \sim \langle\sqrt{A(t)}\rangle$, where $A(t)$ is the area of a domain and angular brackets indicate the ensemble average over the simulation box. This calculation ensures that the fusion is instantaneous. Figure 7(b) is the plot of $r_{eq}(t)$ vs t. The late time behavior of r_{eq} is $t^{1/2}$ (dotted-dashed line), clearly in agreement with the proposed scaling of $t^{1/2}$ for droplet coalescence. Note that we performed similar analysis for the cases discussed in Sec. III A 2. However, r_{eq} still yielded $t^{1/3}$ behavior [see Fig. 5(b)], suggesting a different underlying mechanism for domain coarsening. Furthermore, we substantiated the above arguments by performing simulations at higher interfacial tension between fluids A and B (calculated using the Irving-Kirkwood relation[41]), thereby decreasing the fusion time τ_σ. Under these conditions, the domain coarsening proceeds predominantly via droplet coalescence and the corresponding scaling is $t^{1/2}$ as expected. Figure 8 shows the temporal evolution of domain size $r(t)$ at an interfacial tension $\Gamma_{AB} = 14.14 \pm 0.16$. The predicted scaling agrees with the simulation result which is $r(t) \propto t^{1/2}$.

Table II summarizes the measured and predicted values of growth exponent β for different simulation conditions explored in the present work. For critical mixtures of equal Sc fluids, the phase separation proceeds via spinodal decomposition and the corresponding coarsening mechanism is interface diffusion. Whereas in all other cases, the coarsening mechanism is droplet coalescence.

IV. CONCLUSIONS

We studied Schmidt number effects on phase separation of critical and off-critical mixtures of two immiscible fluids in 2D. The Sc of a fluid is modified by varying either s, the exponent of the dissipative force weight function, or γ, coefficient of the dissipative force or both. In the case of critical mixtures with equal Schmidt number fluids, the phase separation is spinodal decomposition and proceeds via interface diffusion producing a $t^{1/2}$ power law for the domain size. However, for unequal Schmidt number fluids of critical composition, the phase separation is modified qualitatively. At early times, the phase separation resembles a spinodal decomposition which quickly transforms into a droplet coalescence regime. During this regime, the low viscous fluid forms densely populated droplets in the high viscous fluid and the droplets coalesce in time. This gives rise to a $t^{1/3}$ for the domain size which disagrees with the proposed scaling law $t^{1/2}$. Despite the $r(t) \sim t^{1/3}$ behavior, we see *no* evidence of the LSW mechanism. We speculate that the observed scaling behavior $t^{1/3}$ is due to hydrodynamics affecting the droplet coalescence as suggested by Luo *et al.*[19] For the off-critical mixtures, the observed mechanism for domain coarsening is always droplet coalescence. Based of dimensional analysis arguments, the proposed scaling law is $t^{1/2}$ when $\tau_\sigma \ll \tau_D$, where τ_σ is the drop fusion time and τ_D is drop diffusion time. However, the aforementioned inequality breaks down for the choice of our simulation parameters. We circumvented this by calculating the domain size as $r_{eq}(t) \sim \langle\sqrt{A(t)}\rangle$ which makes the droplet fusion instantaneous. Now, the quantity $r_{eq}(t)$ follows the proposed scaling law of $t^{1/2}$ as expected. Moreover, we demonstrated that decreasing τ_σ (by increasing interfacial tension between fluids A and B) yields the correct scaling law, i.e., $t^{1/2}$ for droplet coalescence without the need for calculating r_{eq} confirming the above rationale.

ACKNOWLEDGMENTS

H.G. would like to thank Dr. Vijay Anand for useful discussions. V.S.A. would like to thank Mr. Chandrasekhar Akella for the help with the High Performance Computing Environment Facility at IIT Madras.

REFERENCES

[1] M. Haataja and F. Leonard, Phys. Rev. B **69**, 081201 (2004).
[2] C. Capdevila, M. K. Miller, K. F. Russell, J. Chao, and J. L. Gonzalez-Carrasco, Mater. Sci. Eng.: A **490**, 277 (2008).
[3] B. J. Cherayil, J. Chem. Phys. **96**, 9173 (1992).
[4] P. van de Witte, P. Dijkstra, J. van den Berg, and J. Feijen, J. Membr. Sci. **117**, 1 (1996).
[5] T.-M. Huang, K. McCreary, S. Garg, and T. Kyu, J. Chem. Phys. **134**, 124508 (2011).
[6] R. S. Zola, L. R. Evangelista, Y. C. Yang, and D. K. Yang, Phys. Rev. Lett. **110**, 057801 (2013).
[7] M. Bazec and S. Zumer, Phys. Rev. E **73**, 021703 (2006).
[8] T. Araki and H. Tanaka, Phys. Rev. Lett. **93**, 015702 (2004).
[9] M. S. Miguel, M. Grant, and J. D. Gunton, Phys. Rev. A **31**, 1001 (1985).
[10] K. E. Novik and P. V. Coveney, Phys. Rev. E **61**, 435 (2000).
[11] A. G. Lamorgese and R. Mauri, Phys. Fluids **17**, 034107 (2005).
[12] A. G. Lamorgese and R. Mauri, Int. J. Multiphase Flow **34**, 987 (2008).
[13] R. Shimizu and H. Tanaka, Nat. Commun. **6**, 7407 (2015).
[14] Y. C. Chou and W. I. Goldburg, Phys. Rev. A **20**, 2105 (1979).
[15] N.-C. Wong and C. M. Knobler, Phys. Rev. A **24**, 3205 (1981).
[16] P. J. Hoogerbrugge and J. M. V. A. Koelman, Europhys. Lett. **19**, 155 (1992).
[17] P. Espanol and P. Warren, Europhys. Lett. **30**, 191 (1995).
[18] R. D. Groot and P. B. Warren, J. Chem. Phys. **107**, 4423 (1997).
[19] K. Luo, W. Gronski, and C. Friedrich, Macromol. Theory Simul. **13**, 365 (2004).
[20] A. J. Wagner and J. M. Yeomans, Phys. Rev. Lett. **80**, 1429 (1998).
[21] X. Fan, N. Phan-Thien, N. T. Yong, X. Wu, and D. Xu, Phys. Fluids **15**, 11 (2003).

[22]R. C. Krafnick and A. E. García, J. Chem. Phys. **143**, 243106 (2015).
[23]S. Yaghoubi, E. Shirani, A. R. Pishevar, and Y. Afshar, Europhys. Lett. **110**, 24002 (2015).
[24]A. Lamorgese and R. Mauri, J. Appl. Phys. **121**, 134302 (2017).
[25]A. Onuki, Int. J. Thermophys. **16**, 381 (1995).
[26]H. Tanaka, Phys. Rev. Lett. **71**, 3158 (1993).
[27]H. Tanaka, Phys. Rev. Lett. **76**, 787 (1996).
[28]H. S. Jeon, Z. Shou, A. Chakrabarti, and E. K. Hobbie, Phys. Rev. E **65**, 041508 (2002).
[29]W. Pan, I. V. Pivkin, and G. E. Karniadakis, Europhys. Lett. **84**, 10012 (2008).
[30]X. Fan, N. Phan-Thien, S. Chen, X. Wu, and T. Y. Ng, Phys. Fluids **18**, 063102 (2006).
[31]H. Gidituri, D. V. Anand, S. Vedantam, and M. V. Panchagnula, J. Chem. Phys. **147**, 074703 (2017).
[32]D. Visser, H. Hoefsloot, and P. Iedema, J. Comput. Phys. **214**, 491 (2006).
[33]S. K. Ranjith, B. S. V. Patnaik, and S. Vedantam, J. Comput. Phys. **232**, 174 (2013).
[34]D. Kasiteropoulou, T. Karakasidis, and A. Liakopoulos, Mater. Sci. Eng.: B **176**, 1574 (2011).
[35]R. Yamamoto and K. Nakanishi, Phys. Rev. B **49**, 14958 (1994).
[36]D. A. Huse, Phys. Rev. B **34**, 7845 (1986).
[37]I. Lifshitz and V. Slyozov, J. Phys. Chem. Solids **19**, 35 (1961).
[38]C. Wagner, Elektrochem. Z. **65**, 581 (1961).
[39]P. W. Voorhees, Annu. Rev. Mater. Sci. **22**, 197 (1992).
[40]E. D. Siggia, Phys. Rev. A **20**, 595 (1979).
[41]A. T. Clark, M. Lal, J. N. Ruddock, and P. B. Warren, Langmuir **16**, 6342 (2000).